



## Aberystwyth University

### *Microbial oxidation as a methane sink beneath the West Antarctic Ice Sheet*

Michaud, Alexander B.; Dore, John E.; Achberger, Amanda M.; Christner, Brent C.; Mitchell, Andrew; Skidmore, Mark L.; Vick-Majors, Trista; Priscu, John C.

*Published in:*

Nature Geoscience

*DOI:*

[10.1038/ngeo2992](https://doi.org/10.1038/ngeo2992)

*Publication date:*

2017

*Citation for published version (APA):*

Michaud, A. B., Dore, J. E., Achberger, A. M., Christner, B. C., Mitchell, A., Skidmore, M. L., Vick-Majors, T., & Priscu, J. C. (2017). Microbial oxidation as a methane sink beneath the West Antarctic Ice Sheet. *Nature Geoscience*, 10, 582-586. <https://doi.org/10.1038/ngeo2992>

#### **General rights**

Copyright and moral rights for the publications made accessible in the Aberystwyth Research Portal (the Institutional Repository) are retained by the authors and/or other copyright owners and it is a condition of accessing publications that users recognise and abide by the legal requirements associated with these rights.

- Users may download and print one copy of any publication from the Aberystwyth Research Portal for the purpose of private study or research.
- You may not further distribute the material or use it for any profit-making activity or commercial gain
- You may freely distribute the URL identifying the publication in the Aberystwyth Research Portal

#### **Take down policy**

If you believe that this document breaches copyright please contact us providing details, and we will remove access to the work immediately and investigate your claim.

tel: +44 1970 62 2400  
email: [is@aber.ac.uk](mailto:is@aber.ac.uk)

1 Microbial oxidation as a methane sink beneath the West Antarctic Ice Sheet

2  
3 Alexander B. Michaud<sup>1,†,\*</sup>, John E. Dore<sup>1</sup>, Amanda M. Achberger<sup>2,‡</sup>, Brent C. Christner<sup>2,3</sup>,  
4 Andrew C. Mitchell<sup>4</sup>, Mark L. Skidmore<sup>5</sup>, Trista J. Vick-Majors<sup>1,††</sup>, and John C. Priscu<sup>1,\*</sup>

5  
6 <sup>1</sup> Department of Land Resources and Environmental Sciences, Montana State University,  
7 Bozeman, MT, 59717, USA

8  
9 <sup>2</sup> Department of Biological Sciences, Louisiana State University, Baton Rouge, LA, 70803, USA

10  
11 <sup>3</sup> Department of Microbiology and Cell Science, University of Florida, Gainesville, FL, 32611,  
12 USA

13  
14 <sup>4</sup> Department of Geography and Earth Sciences, Aberystwyth University, Aberystwyth, SY23  
15 3DB, UK

16  
17 <sup>5</sup> Department of Earth Sciences, Montana State University, Bozeman, MT, 59717, USA

18  
19 \* Correspondence to: John C. Priscu, [jpriscu@montana.edu](mailto:jpriscu@montana.edu) or Alexander B. Michaud,  
20 [abmichaud@gmail.com](mailto:abmichaud@gmail.com)

21 † Present Address: Center for Geomicrobiology, Department of Bioscience, Aarhus University,  
22 8000 Aarhus C, DK

23 ‡ Present Address: Department of Oceanography, Texas A&M University, College Station, TX,  
24 77840, USA

25 †† Present Address: Département des Sciences Biologiques, Université du Québec à Montréal,  
26 Case Postale 8888, Succursale Centre-Ville, Montréal, Quebec, Canada H3C 3P8

27 **Summary Paragraph**

28 Aquatic habitats beneath ice masses contain active microbial ecosystems capable of cycling  
29 important greenhouse gases, such as methane (CH<sub>4</sub>). Models suggest that a large methane  
30 reservoir exists beneath the West Antarctic Ice Sheet, but the quantity, source and fate of such  
31 methane remain poorly understood. The availability of O<sub>2</sub> from basal melting of the West  
32 Antarctic Ice Sheet provides conditions favorable for aerobic methane oxidation. Here, we  
33 present measurements of methane concentration and stable isotopic composition from Subglacial  
34 Lake Whillans, which lies beneath the West Antarctic Ice Sheet. We show that sub-ice sheet  
35 methane is produced through the biological reduction of carbon dioxide using H<sub>2</sub>. This methane  
36 pool is subsequently consumed by aerobic, bacterial methane oxidation at the lake sediment-  
37 water interface, a metabolic process supported by the presence of genes involved in methane  
38 oxidation. Bacterial oxidation consumes >99% of the methane and represents a significant  
39 methane sink, and source of biomass carbon and metabolic energy to the surficial SLW  
40 sediments. Our data reveal that aerobic methanotrophy may mitigate the release of methane to  
41 the atmosphere during subglacial water drainage to ice sheet margins and during periods of  
42 deglaciation.

43

44 **Main Text**

45 Methane (CH<sub>4</sub>) is an important greenhouse gas that affects atmospheric chemistry and  
46 radiative balance of Earth. Consequently, understanding its global sources, sinks, and feedbacks  
47 within the climate system is of considerable importance<sup>1</sup>. The primary pathway for biological  
48 CH<sub>4</sub> production in carbon-rich habitats (e.g., bogs, wetlands) is the anaerobic fermentation of  
49 simple organic compounds by certain archaea (acetoclastic or methylotrophic methanogenesis<sup>2</sup>).

50 An alternative microbial pathway to CH<sub>4</sub> production is the reduction of CO<sub>2</sub> coupled to the  
51 oxidation of H<sub>2</sub> (hydrogenotrophic methanogenesis), which is common in anoxic, low sulfate  
52 environments such as the methanogenic zone within marine sediments<sup>2</sup>. Conversely, bacterial  
53 and archaeal oxidation of CH<sub>4</sub> (aerobic and anaerobic, respectively) to CO<sub>2</sub> is a major pathway  
54 that reduces net CH<sub>4</sub> release to the atmosphere<sup>3</sup>.

55 Anoxic habitats in sediments beneath the Antarctic ice sheet may be globally important sites of  
56 biological CH<sub>4</sub> production that could potentially add significant CH<sub>4</sub> to the atmosphere upon  
57 subglacial water drainage to the ice sheet margins or deglaciation<sup>4-6</sup>. However, due to release of  
58 oxygen into the subglacial environment from the overlying ice sheet through geothermal heat-  
59 induced melting<sup>7-9</sup>, aerobic methanotrophic activity can ultimately mitigate CH<sub>4</sub> release to the  
60 atmosphere. We present the first data on CH<sub>4</sub> concentration and stable isotopic composition,  
61 along with genomic data collected from Subglacial Lake Whillans (SLW), which lies ~800 m  
62 beneath the West Antarctic Ice Sheet (WAIS). Collectively, these data reveal the presence of an  
63 ecosystem supported, in part, by active microbial transformations of CH<sub>4</sub>.

64 **Quantity and source of sub ice-sheet CH<sub>4</sub>.** CH<sub>4</sub> concentration in SLW ranged from  
65 0.024 μM in the lake water to 300 μM in the deepest (39 cm) sediment porewater sample (Fig.  
66 1). Fick's first law was used to compute a flux of  $6.8 \pm 1.8$  (mean  $\pm$  SE) mmol CH<sub>4</sub> m<sup>-2</sup> y<sup>-1</sup> into  
67 the surficial sediment (0-2 cm) of SLW using the concentration gradient in the top 15 cm of  
68 sediment and the associated error of the concentration gradient, which includes any potential  
69 sampling artifacts. CH<sub>4</sub> in the SLW sediment had an average δ<sup>13</sup>C-CH<sub>4</sub> value of -74.7‰ (range: -  
70 77.1 to -70.1‰) (Fig. 1) and, together with δD-CH<sub>4</sub> values (range: -247.6 to -239.3‰), reveals  
71 that SLW CH<sub>4</sub> is likely produced by hydrogenotrophic methanogenesis<sup>10</sup> (Fig. 2). This  
72 conclusion contrasts with previous models suggesting that potential CH<sub>4</sub> reservoirs beneath the

73 WAIS would be largely formed through acetoclastic methanogenesis<sup>4</sup>. Hydrogenotrophic  
74 methanogenesis is common in marine sediments and other environments with low concentrations  
75 of old organic carbon, supporting our results from SLW, which also has low organic carbon and  
76 acetate (2-14  $\mu\text{M}$ ) relative to environments with active acetoclastic methanogenesis<sup>10-13</sup>  
77 (Supplementary Fig. 1).  $\text{CO}_2$  for hydrogenotrophic methanogenesis can be supplied from  
78 microbial respiration or bicarbonate in sediment porewater (2-6  $\text{mM}$ )<sup>14</sup>, and hydrogen can be  
79 generated abiotically from glacially-crushed siliceous bedrock, radiolysis of water, hydrothermal  
80 input, or biologically via fermentation<sup>2,8,15,16</sup>. Attempts to amplify a marker gene for  
81 methanogenic archaea (*mcrA*)<sup>17,18</sup> from the 0-2, 4-6, 18-20 and 34-36 cm depth intervals within  
82 the SLW sediment core were unsuccessful, implying that the abundance of methanogenic  
83 archaea was low or below detection. A community analysis of 16S rRNA molecules, which  
84 indicates the potentially active fraction of the microbial community<sup>19,20</sup>, showed relatives of  
85 methanogenic species (i.e., *Methanohalophilus levihalophilus*) were rare members (0.1%) of the  
86 active sediment community at 35 cm depth (Fig. 1B)<sup>21</sup>. The most parsimonious explanation for  
87 our concentration profile and molecular microbiological results is the presence of a  
88 contemporary or relict  $\text{CH}_4$  source that originates from depths below our deepest sample and  
89 diffuses towards an aerobic methanotrophic sink at the sediment-water interface.

90 **Active aerobic methanotrophy.** The low water column  $\text{CH}_4$  concentration, relative to  
91 the sediment porewater, and the decrease in  $\text{CH}_4$  concentration in the upper ~16 cm of sediment  
92 indicate that  $\text{CH}_4$  oxidation consumes almost all (>99%) of the upwardly diffusing sedimentary  
93  $\text{CH}_4$  (Fig. 1A). The four order of magnitude decrease in  $\text{CH}_4$  concentration from the surficial  
94 sediments to the water column corresponds with a large, positive shift (30.7‰) in the  $\delta^{13}\text{C}\text{-CH}_4$   
95 (Fig. 1A). We used the Rayleigh distillation model to calculate a kinetic isotope fractionation

96 factor (KIFF) of  $\alpha = 1.004$  associated with the  $\text{CH}_4$  oxidation process<sup>22</sup>. This model assumes a  
97 closed system (i.e., no other inputs of  $\text{CH}_4$  and measured isotope values are not affected by  
98 mixing) and that the only sink for sediment  $\text{CH}_4$  is bacterial oxidation. The KIFF calculated for  
99  $\text{CH}_4$  oxidation in SLW is within the lower range of those derived from laboratory cultures, but is  
100 similar to estimates from field measurements made in cold, marine habitats ( $\alpha = 1.003 -$   
101  $1.035$ )<sup>22,23</sup>. The observed fractionation in SLW is consistent with near-complete removal of  
102 upwardly diffusing sedimentary  $\text{CH}_4$  by aerobic  $\text{CH}_4$  oxidizing bacteria<sup>23</sup>.

103 We amplified the  $\beta$ -subunit of the particulate methane monooxygenase gene (*pmoA*)  
104 found in aerobic  $\text{CH}_4$  oxidizing bacteria to further evaluate the functional potential for  $\text{CH}_4$   
105 oxidation. Results revealed that *pmoA* was detectable in the water column and the upper 16 cm  
106 of sediment, but not in deeper layers of the core. The presence of *pmoA* genes is consistent with  
107 measured  $\text{O}_2$  concentration of  $71.9 \mu\text{M}$ , in SLW lake waters<sup>1</sup>, and redox-sensitive trace metal  
108 abundance in the sediment core that implies the presence of  $\text{O}_2$  to a depth of  $\sim 16 \text{ cm}$ <sup>14</sup>. Thus, the  
109 functional potential for aerobic methanotrophy (*pmoA* gene presence) occurs where both  $\text{CH}_4$   
110 and  $\text{O}_2$  are available. SLW *pmoA* sequences were similar ( $>87\%$  DNA similarity) to  
111 *Methylobacter tundripaludum*, an aerobic  $\text{CH}_4$  oxidizing bacterium (Fig. 3). *M. tundripaludum*  
112 was also the closest described and cultured phylogenetic relative (99% rDNA gene sequence  
113 similarity) to the putative  $\text{CH}_4$  oxidizing taxa recovered from 16S rDNA gene sequence analysis  
114 of the SLW microbial community (Fig. 3; OTU 000112)<sup>7,21</sup>. The *pmoA* sequences present in  
115 SLW were related to *pmoA* sequences collected from an active  $\text{CH}_4$  oxidizing environment at the  
116 margin of the Greenland Ice Sheet (Fig. 3)<sup>5</sup>. Although the *pmoA* primer set we used was  
117 designed to detect a wide diversity of methanotrophs<sup>24</sup>, additional putative methanotrophic

118 genera were detected in the 16S rDNA and rRNA community analysis (Supplementary Fig. 1),  
119 but these genera were at least one order of magnitude less abundant than *M. tundripaludum*.

120 Aerobic CH<sub>4</sub> oxidizing bacteria are typically members of the *Gammaproteobacteria* and  
121 *Alphaproteobacteria*<sup>25</sup> and further classified into different types based on the substrate affinity of  
122 their methane monooxygenase enzyme<sup>25</sup>. Type Ia *Gammaproteobacteria* methanotrophs have  
123 methane monooxygenase enzymes with low affinity for CH<sub>4</sub> while type II *Alphaproteobacteria*  
124 have enzymes with a high affinity for CH<sub>4</sub><sup>26</sup>. These type Ia *Gammaproteobacteria*  
125 methanotrophs, particularly *Methylobacter* sp., dominate the active fraction of methanotroph  
126 populations in freshwater environments that have high CH<sub>4</sub> (μM – mM) concentrations and  
127 strong CH<sub>4</sub> sources<sup>25,26</sup>. *M. tundripaludum* possesses a low affinity (type Ia) methane  
128 monooxygenase enzyme, is known to be cold-adapted<sup>24,26</sup>, has been shown to be active at the  
129 Greenland Ice Sheet margin<sup>5</sup> and is responsible for significant CH<sub>4</sub> consumption in a variety of  
130 other Arctic habitats<sup>27–29</sup>. Both the low CH<sub>4</sub> affinity and temperature adaptation of the type Ia  
131 *Gammaproteobacteria* particulate methane monooxygenase enzyme reflect the conditions  
132 measured in SLW (-0.5°C and 0.1 to 0.3 mM CH<sub>4</sub>; Fig. 1)<sup>9</sup>. Indeed, a community analysis of 16S  
133 rRNA molecules showed *M. tundripaludum* and other methanotrophic taxa were abundant  
134 (≥1.0%) in the water column and upper sediments (0-6 cm), with their greatest relative  
135 abundance in the surficial sediments (16%; Fig. 1B; Supplementary Fig. 1)<sup>21</sup>. These molecular  
136 data, based on *pmoA* gene sequences and 16S rRNA molecules, indicate that methanotrophs  
137 related to *M. tundripaludum* are abundant and potentially metabolically active near the SLW  
138 sediment-water interface, where geochemical data indicate peak methane oxidation.

139 **The role of CH<sub>4</sub> in the subglacial ecosystem.** We computed chemical affinity ( $A_r$ ) for  
140 the surficial (0-2 cm) sediment layer to estimate the available biochemical energy from CH<sub>4</sub>

141 oxidation compared to other potential metabolic reactions<sup>30,31</sup> (Fig. 4). O<sub>2</sub> concentration data in  
 142 the surficial sediment layer are not available, so biochemical reactions were modeled at half  
 143 (36.5 μM) and one-tenth (7.3 μM) of the average SLW water column O<sub>2</sub> concentration. These  
 144 modeled O<sub>2</sub> concentrations are reasonable given the evidence for O<sub>2</sub> penetration to ~16 cm<sup>14</sup>.  
 145 While pyrite and ammonium oxidation are predicted to yield the greatest metabolic energy in the  
 146 water column<sup>32</sup>, aerobic CH<sub>4</sub> oxidation is the most exergonic biochemical pathway in the  
 147 surficial sediment despite the modeled 10-fold reduction in O<sub>2</sub> concentration relative to lake  
 148 water (A<sub>r</sub><sup>e-</sup>: 99.9 kJ mol e<sup>-</sup><sup>-1</sup>; A<sub>r</sub><sup>kg</sup>: 2.84 J kg H<sub>2</sub>O<sup>-1</sup>) (Fig. 4). The microbial community  
 149 composition reflects the chemical affinity calculations such that iron, sulfide and ammonium  
 150 oxidizing taxa are abundant in the water column<sup>21,32</sup> and aerobic methane oxidizing taxa are  
 151 abundant and active in the surficial sediment (Fig. 1). These chemical affinity calculations  
 152 corroborate the molecular and geochemical data by showing sufficient biochemical energy is  
 153 present in the SLW surficial sediment to support the abundant methanotroph population (Fig. 4).

154 We modeled the rate of biological CH<sub>4</sub> consumption in SLW as;

$$155 \quad \frac{dC}{dt} = (F_{diff} \times A) - (R \times V) \quad (1)$$

156 where,  $\frac{dC}{dt}$  is the change in CH<sub>4</sub> concentration over time,  $F_{diff}$  is the diffusional flux into the 0-2  
 157 cm surficial sediment, A is the area of SLW, R is the rate of CH<sub>4</sub> consumption, and V is volume  
 158 of SLW plus the porewater surficial sediment. Assuming steady-state conditions (i.e.,  $\frac{dC}{dt} = 0$ ),  
 159 equation (1) can be rewritten as:

$$160 \quad R = \frac{F_{diff}}{H_L + (H_{SS} \times \varphi)} \quad (2)$$

161 where, H<sub>L</sub> and H<sub>SS</sub> are the height of the lake and surficial (0-2 cm) sediments, respectively, and φ  
 162 is the sediment porosity. R equates to 3.0 ± 0.8 mmol CH<sub>4</sub> m<sup>-3</sup> y<sup>-1</sup>. The rate of CH<sub>4</sub> removal (R)



163 is the sum of both CH<sub>4</sub> oxidation ( $R_{ox}$ ) and incorporation of CH<sub>4</sub> as a carbon source ( $R_{incorp}$ ) for  
164 microbial biomass synthesis. Using the total CH<sub>4</sub> removal rate ( $R$ ), together with the average  
165 fraction of CH<sub>4</sub> (~0.5) partitioned to biomass formation for type I methanotrophs<sup>33</sup>, reveals that  
166 methanotrophs may oxidize 1.5 mmol CH<sub>4</sub> m<sup>-3</sup> y<sup>-1</sup> to CO<sub>2</sub> ( $R_{ox}$ ) and assimilate 1.5 mmol CH<sub>4</sub> m<sup>-3</sup>  
167 y<sup>-1</sup> ( $R_{incorp}$ ) as a biosynthetic carbon source (Supplementary Table 1). Given 0.5 as a biomass  
168 partitioning factor, the rate of aerobic CH<sub>4</sub> oxidation would be 10 to 100-fold lower than aerobic  
169 CH<sub>4</sub> oxidation measured in cold (~4°C), surficial marine sediments and deep sea, CH<sub>4</sub> seeps<sup>34,35</sup>.  
170 The biomass partitioning factor can vary from 0.06 to 0.7 in lakes with active methanotrophy<sup>36</sup>.  
171 When we account for this potential variability in the biomass partitioning factor and the  
172 uncertainty in the CH<sub>4</sub> flux,  $R_{ox}$  and  $R_{incorp}$  vary by an order of magnitude; the range of  $R_{incorp}$  is  
173 0.14 – 3.0 mmol CH<sub>4</sub> m<sup>-3</sup> y<sup>-1</sup> and the  $R_{ox}$  is 0.52 – 3.6 mmol CH<sub>4</sub> m<sup>-3</sup> y<sup>-1</sup> (Supplementary Table  
174 1). It is important to note that  $R_{ox}$  and  $R_{incorp}$  are inversely related (Supplementary Table 1).  
175 While the overall rate of oxidation may be low compared to marine sediment methanotrophy, if  
176 the formation of biomass due to CH<sub>4</sub> oxidation occurred solely in the surficial SLW sediment  
177 porewaters, where molecular data indicate peak active methanotroph abundance (Fig. 1B), the  
178 biosynthetic rate would be 26.2 ng C (L porewater)<sup>-1</sup> d<sup>-1</sup> (range: 2.3 – 51 ng C (L porewater)<sup>-1</sup> d<sup>-1</sup>;  
179 Supplementary Table 1). This modeled biomass C production rate via sedimentary  
180 methanotrophy is nearly equivalent (80%; range: 7 - 155%) to measured rates of  
181 chemoautotrophic biomass C production (32.9 ng C L<sup>-1</sup> d<sup>-1</sup>) within the SLW water column<sup>7</sup>.  
182 These results indicate that CH<sub>4</sub>, as modeled, is an important carbon and energy source for the  
183 SLW sediment microbial community.

184 The O<sub>2</sub> demand derived from the modeled CH<sub>4</sub> removal rate ( $R$ ) is 6.1 x 10<sup>5</sup> mol O<sub>2</sub> y<sup>-1</sup>,  
185 using 0.5 as the biomass partitioning factor. Methanotrophy in SLW is responsible for

186 consuming ~16% (range: 10 – 24%; Supplementary Table 1) of the O<sub>2</sub> supply to the SLW  
187 ecosystem<sup>32</sup>. Thus, the impact of oxygen demand due to CH<sub>4</sub> oxidation in the SLW ecosystem  
188 depends on the balance between methanotroph growth and energy requirements. Despite a  
189 potentially large range in the biomass partitioning factor, these calculations show that O<sub>2</sub>  
190 released from basal melting of the overlying ice sheet fuels an abundant and active population of  
191 methanotrophs in the lake. Saturated sediments at SLW are similar in nature to those found  
192 beneath other ice streams of the Siple coast region (e.g., ref. 8) and basal ice melt is extensive  
193 beneath the WAIS<sup>37,38</sup>, which may produce extensive oxic subglacial aquatic habitats, conducive  
194 to cosmopolitan populations of methanotrophs that convert CH<sub>4</sub> to CO<sub>2</sub> and biomass.

195         Our data reveal that hydrogenotrophic methanogenesis is the main pathway of CH<sub>4</sub>  
196 formation beneath SLW and that CH<sub>4</sub> is utilized by aerobic methanotrophic bacteria. Contrary to  
197 previous predictions which suggested the potential significance of subglacial CH<sub>4</sub> fluxes to the  
198 atmosphere (e.g., ref. 4), our CH<sub>4</sub> measurements and flux calculations show that aerobic  
199 methanotrophic bacteria in SLW convert most (>99%) of the sedimentary CH<sub>4</sub> efflux to CO<sub>2</sub> and  
200 biomass. The bacterial conversion of CH<sub>4</sub> to CO<sub>2</sub> beneath the WAIS reduces the warming  
201 potential of subglacial gases<sup>39</sup> that may be released to downstream ice sheet margin  
202 environments and to the atmosphere during episodes of ice sheet retreat. Given the potential for  
203 widespread hydrogenotrophic CH<sub>4</sub> production in sediments beneath ice sheets, such as the  
204 WAIS, and the release of O<sub>2</sub> due to melting at the ice sheet base<sup>9,37,38</sup>, biological transformations  
205 of CH<sub>4</sub> may be significant for the functioning and persistence of deep microbial life and  
206 biogeochemical processes in Antarctic sub-ice environments.

207 **References**

- 208 1. Kirschke, S. *et al.* Three decades of global methane sources and sinks. *Nat. Geosci.* **6**,  
209 813–823 (2013).
- 210 2. Thauer, R. K., Kaster, A.-K., Seedorf, H., Buckel, W. & Hedderich, R. Methanogenic  
211 archaea: ecologically relevant differences in energy conservation. *Nat. Rev. Microbiol.* **6**,  
212 579–91 (2008).
- 213 3. Conrad, R. The global methane cycle: recent advances in understanding the microbial  
214 processes involved. *Environ. Microbiol. Rep.* **1**, 285–92 (2009).
- 215 4. Wadham, J. L. *et al.* Potential methane reservoirs beneath Antarctica. *Nature* **488**, 633–  
216 637 (2012).
- 217 5. Dieser, M. *et al.* Molecular and biogeochemical evidence for methane cycling beneath the  
218 western margin of the Greenland Ice Sheet. *ISME J.* **8**, 2305–2316 (2014).
- 219 6. Wadham, J. L. *et al.* The potential role of the Antarctic Ice Sheet in global biogeochemical  
220 cycles. *Earth Environ. Sci. Trans. R. Soc. Edinburgh* **104**, 55–67 (2013).
- 221 7. Christner, B. C. *et al.* A microbial ecosystem beneath the West Antarctic ice sheet. *Nature*  
222 **512**, 310–313 (2014).
- 223 8. Skidmore, M. in *Antarctic Subglacial Environments, Geophysical Monograph Series* (eds.  
224 Siebert, M. J., Kennicutt II, M. C. & Bindschandler, R. A.) 61–81 (American Geophysical  
225 Union, 2011).
- 226 9. Fisher, A. T., Mankoff, K. D., Tulaczyk, S. M. & Tyler, S. W. High geothermal heat flux  
227 measured below the West Antarctic Ice Sheet. *Sci. Reports* **1**, 1–9 (2015).
- 228 10. Whiticar, M. J. Carbon and hydrogen isotope systematics of bacterial formation and  
229 oxidation of methane. *Chem. Geol.* **161**, 291–314 (1999).

- 230 11. Coleman, D. D., Liu, C.-L. & Riley, K. M. Microbial methane in the shallow Paleozoic  
231 sediments and glacial deposits of Illinois, U.S.A. *Chem. Geol.* **71**, 23–40 (1988).
- 232 12. Conrad, R. in *Advances in Agronomy* (ed. Sparks, S.) 1–63 (Elsevier, 2007).
- 233 13. Schoell, M. Multiple origins of methane in the Earth. *Chem. Geol.* **71**, 1–10 (1988).
- 234 14. Michaud, A. B. *et al.* Solute sources and geochemical processes in Subglacial Lake  
235 Whillans, West Antarctica. *Geology* **44**, 347–350 (2016).
- 236 15. Telling, J. *et al.* Rock comminution as a source of hydrogen for subglacial ecosystems.  
237 *Nat. Geosci.* **8**, 851–855 (2015).
- 238 16. Lin, L.-H., Slater, G. F., Sherwood Lollar, B., Lacrampe-Couloume, G. & Onstott, T. C.  
239 The yield and isotopic composition of radiolytic H<sub>2</sub>, a potential energy source for the deep  
240 subsurface biosphere. *Geochim. Cosmochim. Acta* **69**, 893–903 (2005).
- 241 17. Matheus Carnevali, P. B. *et al.* Methane sources in arctic thermokarst lake sediments on  
242 the North Slope of Alaska. *Geobiology* **13**, 181–197 (2015).
- 243 18. Lever, M. A. *et al.* Evidence for microbial carbon and sulfur cycling in deeply buried  
244 ridge flank basalt. *Science*. **339**, 1305–1308 (2013).
- 245 19. Blazewicz, S. J., Barnard, R. L., Daly, R. A. & Firestone, M. K. Evaluating rRNA as an  
246 indicator of microbial activity in environmental communities: limitations and uses. *ISME*  
247 *J.* **7**, 2061–2068 (2013).
- 248 20. Jones, S. E. & Lennon, J. T. Dormancy contributes to the maintenance of microbial  
249 diversity. *Proc. Natl. Acad.* **107**, 5881–5886 (2010).
- 250 21. Achberger, A. M. *et al.* Microbial community structure of Subglacial Lake Whillans, West  
251 Antarctica. *Front. Microbiol.* **7**, 1–13 (2016).
- 252 22. Grant, N. J. & Whiticar, M. J. Stable carbon isotopic evidence for methane oxidation in

- 253 plumes above Hydrate Ridge, Cascadia Oregon Margin. *Global Biogeochem. Cycles* **16**,  
254 1–13 (2002).
- 255 23. Coleman, D. D., Risatti, J. B. & Schoell, M. Fractionation of carbon and hydrogen  
256 isotopes by methane-oxidizing bacteria. *Geochim. Cosmochim. Acta* **45**, 1033–1037  
257 (1981).
- 258 24. McDonald, I. R., Bodrossy, L., Chen, Y. & Murrell, J. C. Molecular ecology techniques  
259 for the study of aerobic methanotrophs. *Appl. Environ. Microbiol.* **74**, 1305–15 (2008).
- 260 25. Knief, C. Diversity and habitat preferences of cultivated and uncultivated aerobic  
261 methanotrophic bacteria evaluated based on pmoA as molecular marker. *Front. Microbiol.*  
262 **6**, 1346 (2015).
- 263 26. Ho, A. *et al.* Conceptualizing functional traits and ecological characteristics of methane-  
264 oxidizing bacteria as life strategies. *Environ. Microbiol. Rep.* **5**, 335–345 (2013).
- 265 27. Martineau, C., Whyte, L. G. & Greer, C. W. Stable isotope probing analysis of the  
266 diversity and activity of methanotrophic bacteria in soils from the Canadian high Arctic.  
267 *Appl. Environ. Microbiol.* **76**, 5773–84 (2010).
- 268 28. Graef, C., Hestnes, A. G., Svenning, M. M. & Frenzel, P. The active methanotrophic  
269 community in a wetland from the High Arctic. *Environ. Microbiol. Rep.* **3**, 466–472  
270 (2011).
- 271 29. He, R. *et al.* Shifts in identity and activity of methanotrophs in Arctic lake sediments in  
272 response to temperature changes. *Appl. Environ. Microbiol.* **78**, 4715–4723 (2012).
- 273 30. Shock, E. L. *et al.* Quantifying inorganic sources of geochemical energy in hydrothermal  
274 ecosystems, Yellowstone National Park, USA. *Geochim. Cosmochim. Acta* **74**, 4005–4043  
275 (2010).

- 276 31. Amend, J. P. & Shock, E. L. Energetics of overall metabolic reactions of thermophilic and  
277 hyperthermophilic Archaea and Bacteria. *FEMS Microbiol. Rev.* **25**, 175–243 (2001).
- 278 32. Vick-Majors, T. J. *et al.* Physiological ecology of microorganisms in Subglacial Lake  
279 Whillans. *Front. Microbiol.* **7**, 1-16 (2016).
- 280 33. Trimmer, M. *et al.* Riverbed methanotrophy sustained by high carbon conversion  
281 efficiency. *ISME J.* **9**, 2304–2314 (2015).
- 282 34. Iversen, N. & Blackburn, T. H. Seasonal rates of methane oxidation in anoxic marine  
283 sediments. *Appl. Environ. Microbiol.* **41**, 1295–1300 (1981).
- 284 35. Marlow, J. J. *et al.* Carbonate-hosted methanotrophy represents an unrecognized methane  
285 sink in the deep sea. *Nat. Commun.* **5**, 5094 (2014).
- 286 36. Bastviken, D., Ejlertsson, J., Sundh, I. & Tranvik, L. Methane as a source of carbon and  
287 energy for lake pelagic food webs. *Ecology* **84**, 969–981 (2003).
- 288 37. Lough, A. C. *et al.* Seismic detection of an active subglacial magmatic complex in Marie  
289 Byrd Land, Antarctica. *Nat. Geosci.* **6**, 1031–1035 (2013).
- 290 38. Beem, L. H., Jezek, K. C. & Van Der Veen, C. J. Basal melt rates beneath Whillans Ice  
291 Stream, West Antarctica. *J. Glaciol.* **56**, 647–654 (2010).
- 292 39. Yvon-Durocher, G. *et al.* Methane fluxes show consistent temperature dependence across  
293 microbial to ecosystem scales. *Nature* **507**, 488–91 (2014).

294

295 Correspondence and requests for materials should be addressed to A.B.M or J.P.

296

## 297 **Acknowledgments**

298 This study was funded by National Science Foundation – Division of Polar Programs

299 grants (0838933, 1346250, 1439774 to J.C.P; 0838941 to B.C.C) awarded as part of the Whillans  
300 Ice Stream Subglacial Access Research Drilling (WISSARD) project. We thank the WISSARD  
301 Science Team (see wissard.org for full list of team members) for their assistance in expedition  
302 planning and with collecting and processing samples. Partial support was provided by graduate  
303 fellowships from the NSF-IGERT Program (0654336), Montana Space Grant Consortium and  
304 NSF-Center for Dark Energy Biosphere Investigations (A.B.M); a dissertation grant from the  
305 American Association of University Women (T.J.V-M); a NSF-Graduate Research Fellowship  
306 (A.M.A); and a Sêr Cymru National Research Network for Low Carbon, Energy and the  
307 Environment Grant from the Welsh Government and Higher Education Funding Council for  
308 Wales (A.C.M). We thank R. Scherer and R. Powell for sediment cores. B.B Jørgensen, M.A.  
309 Lever and S. Nielsen provided support and assistance with DNA extraction and *pmoA/mcrA*  
310 amplification. Logistics were conducted by the 139th Expeditionary Airlift Squadron of the New  
311 York Air National Guard, Kenn Borek Air, and Antarctic Support Contractor, managed by  
312 Lockheed-Martin. Hot-water drill support was provided by University of Nebraska-Lincoln and  
313 directed by F. Rack and D. Duling (chief driller). D. Blythe, J. Burnett, C. Carpenter, D. Gibson,  
314 J. Lemery, A. Melby, and G. Roberts provided drill support at SLW. This is C-DEBI  
315 contribution #371.

316

317 **Author Contributions**

318 A.B.M, J.E.D, T.J.V-M, J.C.P and M.L.S wrote the manuscript. A.B.M., J.E.D., M.L.S, and  
319 T.J.V-M. conducted and analyzed methane concentration and isotopic data. A.M.A., A.B.M., and  
320 B.C.C. processed, analyzed and interpreted the molecular data. A.C.M conducted  
321 thermodynamic calculations. All authors contributed to the study design, collection of samples  
322 and approved the final draft of the manuscript.

323

324 **Competing Financial Interests**

325 The authors declare no competing financial interests.

326



327 **Figure Captions**

328 **Figure 1** SLW water column and sediment profile of CH<sub>4</sub> concentration and stable isotope  
329 composition and abundance of active methane oxidizing and methanogenic taxa. **(a)** CH<sub>4</sub>  
330 concentration and  $\delta^{13}\text{C-CH}_4$  values, **(b)** percent relative abundance of known CH<sub>4</sub> oxidizing and  
331 methanogenic bacterial and archaeal taxa, respectively, from the community analysis of 16S  
332 rRNA molecules (note log scale; panel b modified from ref. 21). Dashed lines indicate running  
333 averages using a Loess smoothing function (a). SLW water column values for CH<sub>4</sub> concentration  
334 and stable isotope values are displayed next to points (a). Asterisks indicate that methanogenic  
335 (red) and methanotrophic (black) genera were not detected (b).

336

337 **Figure 2** CH<sub>4</sub> stable isotope biplot for nine depths of the SLW sediment porewater (black  
338 triangles). The shaded areas delineate microbial and thermogenic endmembers as well as regions  
339 of mixed sources (endmember fields modified from ref. 10).  $\delta^{13}\text{C-CH}_4$  values in this plot are the  
340 same as Fig. 1A.

341

342 **Figure 3** Neighbor-joining phylogenetic tree of SLW *pmoA* DNA sequences. *pmoA* sequences  
343 from SLW water column and sediment are highlighted in grey and brackets indicate the number  
344 of sequenced clones within each operational taxonomic unit (OTU) with sequence accession  
345 numbers are shown in parentheses. All solid line branches are *pmoA* sequences of the  
346 *Gammaproteobacteria* type Ia group, including *Methylobacter tundripaludum* (bold), an active  
347 and abundant member of the SLW community<sup>1,17</sup>. Bootstrap support is displayed at branch  
348 points (% , 1000 replications), with values >50% shown. Branch lengths are measured in number  
349 of substitutions per site. The scale bar represents 0.05 substitutions per site.

350

351 **Figure 4** Chemical affinity calculations for the SLW surficial (0-2 cm) sediment. Results are  
352 presented in energy density of joules per kg of water ( $\text{J kg H}_2\text{O}^{-1}$ ; top axis in log scale) and  
353 kilojoules per mole of electron transferred ( $\text{kJ mol e}^{-1}$ ; bottom axis) at 50% (0.5) and 10% (0.1)  
354 of the SLW lake water  $\text{O}_2$  concentration for eight environmentally relevant biochemical  
355 reactions.

356

### 357 **Methods**

358 **Sample Collection.** We used a microbiologically-clean hot water drill to directly sample  
359 the water column and the upper 40 cm of sediment of Subglacial Lake Whillans (SLW;  $84.240^\circ$   
360 S,  $153.694^\circ$  W) to assess the  $\text{CH}_4$  dynamics<sup>40,41</sup>. SLW water column and sediment were sampled  
361 through a 800 m deep,  $\sim 0.6$  m diameter borehole on 30 January 2013. The clean access hot water  
362 drill system has been shown to reduce cell concentrations within the drilling water to  $<100$  cell  
363  $\text{mL}^{-1}$ , which is acceptable based on the predicted cell concentration in the lake water and the  
364 National Research Council 2007 report on subglacial lake access<sup>40,45</sup>. The 2.2 m deep SLW water  
365 column was sampled with a 10 L Niskin bottle, suspended microbial cells were concentrated  
366 using an *in situ* water filtration system and surficial sediments were collected with a gravity  
367 multicorer (60 cm long x 6 cm diameter). For complete drilling and sampling details see ref. 40,  
368 41.

369 **Geochemical Analysis.** Sediment from a gravity core (MC-2A) was sampled every 2 cm  
370 by extrusion and subsampling of each newly exposed layer. Sediment subsamples for methane  
371 ( $\text{CH}_4$ ) were collected using a sterile cut-off 5 ml syringe and immediately placed into 20 ml  
372 sterile serum vials and stoppered with a sterile butyl rubber stopper, then crimped with an

373 aluminum cap. Three empty vials were sealed in the field to capture atmospheric air as  
374 procedural blanks. Ten ml of 2.5% NaOH was added by sterile syringe to each sample vial and  
375 the three blanks, stopping biological activity and creating a pressurized headspace within each  
376 vial<sup>42</sup>. A CH<sub>4</sub> sample from the SLW water column was collected from cast 1 from a Niskin bottle  
377 by placing the tube to the bottom of the serum vial and filling from top to bottom. The water  
378 sample was fixed with Lugol's solution to prevent biological activity. All vials were stored  
379 inverted at 4°C for transport back to Montana State University (MSU) for CH<sub>4</sub> quantification.  
380 Headspace CH<sub>4</sub> was quantified on a Hewlett-Packard 5890 Series II gas chromatograph (GC)  
381 equipped with a flame ionization detector (FID) with a detection limit of 3 nM for water column  
382 samples and 190 nM for the sediment samples. Headspace gas was introduced to the GC using a  
383 10-port injection valve configured for back flushing of a precolumn (25 cm x 0.32 cm OD,  
384 packed with Porapak-T 80/100 mesh) to prevent water vapor from reaching the analytical  
385 columns. The vial overpressure was used to flush and fill a 1 cm<sup>3</sup> sample loop using a syringe  
386 needle inlet; measured laboratory air temperature and pressure were used to calculate the total  
387 moles of gas contained within the loop, assuming gas ideality. Gases were separated on two  
388 analytical columns in series (both 183 cm x 0.32 cm OD, packed with Chromosorb 102 80/100  
389 mesh and Porapak-Q 80/100 mesh, respectively). The columns were maintained at 55°C and the  
390 FID at 240°C. The carrier gas was an ultra-high purity N<sub>2</sub>, which was further purified through  
391 Molecular Sieve 5A, activated charcoal and an O<sub>2</sub> scrubber. The carrier flow was 30 mL min<sup>-1</sup>;  
392 under these conditions, CH<sub>4</sub> eluted to the FID at 1.97 min. Instrument calibration was performed  
393 using certified 500 and 51 ppmv CH<sub>4</sub> in air standards (Air Liquide; ±1% accuracy), and  
394 volumetric dilutions thereof into carrier N<sub>2</sub>. Dissolved CH<sub>4</sub> concentrations were calculated using  
395 Henry's Law based on measured headspace mole fractions and Bunsen solubility coefficients

396 estimated from temperature and sample salinity (including added NaOH) as parameterized by  
397 ref. 46. Porewater volumes were determined from mass loss after drying the sediment at 95°C  
398 until the mass stopped decreasing (~24h), and dry sediment volume was similarly determined  
399 assuming a density of 2.60 g cm<sup>-3</sup> for the sedimentary particles<sup>47</sup>. The total volume of the vials  
400 was determined weighing the vials with sediment and NaOH fixative, then completely filling the  
401 headspace with deionized water and weighing again. The headspace volume was determined by  
402 difference. The extent of pressurization of the headspace was determined from total headspace  
403 volume and the volume of NaOH solution added. The total CH<sub>4</sub> within each vial, after correction  
404 for the small amount of CH<sub>4</sub> present in the headspace air when originally sealed (characterized  
405 by the blank vials), was then used to determine the initial CH<sub>4</sub> concentration of the porewater.

406 Gravity core MC-3A was collected from SLW, capped and immediately frozen (-20°C).  
407 The frozen core was returned to MSU and thawed at 4°C overnight in a class 1000 clean, cold  
408 room in the MSU SubZero Science and Engineering Facility. The core was extruded and cut  
409 every 2 cm and sediment for CH<sub>4</sub> stable isotope analysis was subsampled and fixed using the  
410 same method as for CH<sub>4</sub> concentration analysis from MC-2A described above. One ml of room  
411 temperature headspace gas from the fixed sediment vials was transferred to a gas-tight laminated  
412 foil bag using a gas-tight, glass syringe and diluted 1:100 with CH<sub>4</sub>-free (zero grade) air. The bag  
413 was connected to the inlet of a Picarro G2201-*i* Cavity Ring-Down Spectrometer (CRDS)  
414 specific for high-precision concentration and δ<sup>13</sup>C analyses of CH<sub>4</sub>. Sample was introduced to  
415 the instrument at a flow rate of 100 ml min<sup>-1</sup>; δ<sup>13</sup>C-CH<sub>4</sub> values were determined using factory  
416 calibrations and were averaged over ≥30 s of 1 Hz measurements. Between samples, atmospheric  
417 air was measured for at least 5 min to ensure lack of instrument drift. The δD-CH<sub>4</sub> values were  
418 measured at the University of California Davis Stable Isotope Facility (UCD-SIF) using a

419 PreCon concentration system (ThermoScientific) in line with a Delta V plus isotope ratio mass  
420 spectrometer (ThermoScientific)<sup>43</sup>. Two  $\delta^{13}\text{C}$ -CH<sub>4</sub> samples (MC-3A samples from 18-20 cm and  
421 34-36 cm depths) were also run at UCD-SIF to compare their independent results with our values  
422 obtained on the Picarro CRDS. There was a <4% difference in the  $\delta^{13}\text{C}$ -CH<sub>4</sub> values reported  
423 from the two methods. The carbon and hydrogen stable isotope ratios are reported in  $\delta$ -notation  
424 ( $\delta^{13}\text{C}$ ,  $\delta\text{D}$ ) with respect to VPDB and VSMOW standards, respectively. The running average  
425 (with depth) of the CH<sub>4</sub> concentration and isotope values was calculated in SigmaPlot version 11  
426 using a locally estimated scatterplot smoothing (loess) function with smoothing parameters set to  
427 first degree polynomial and a sampling frequency of 0.45, which determines the number of local  
428 data points used in the weighted regression carried out by the loess smoothing function.

429         Sediments used for dissolved NH<sub>4</sub><sup>+</sup> concentration measurements were collected from  
430 MC-3A<sup>48</sup>. The sediment was transferred to acid washed (10% HCl), ultra-pure water-rinsed  
431 (6X), combusted (4h at 450 °C) glass vials with polytetrafluoroethylene lined caps, frozen at -20  
432 °C and thawed prior to analysis. Sediments were transferred from the glass vials to acid washed  
433 and ultra-pure water rinsed 50 mL conical centrifuge tubes and centrifuged at 3500 x g for 20  
434 minutes. The supernatant was transferred to acid washed and ultra-pure water rinsed 15 mL  
435 conical centrifuge tubes and spun for an additional 20 min at 4500 x g to pellet fine particulates.  
436 The clean supernatant from the 15 mL centrifuge tube was transferred to an acid washed and  
437 ultra-pure water rinsed glass vial. The supernatant was diluted (1:10) to a final volume of 5 mL  
438 with ultra-pure water for colorimetric analysis<sup>49</sup>.

439         Particulate organic carbon and nitrogen values were determined with an elemental  
440 analyzer as described in ref 1. Acetate, formate and oxalate concentrations were determined  
441 using ion chromatography following methods in ref. 14.

442           **Molecular Analyses.** DNA was extracted using a modular method to allow for  
443 optimization of the DNA extraction procedure, specific to the SLW sediments<sup>44</sup>. DNA extraction  
444 yield from SLW sediments was greatest when sediments were pre-treated with 450  $\mu\text{mol g}^{-1}$   
445 deoxynucleotide triphosphate to prevent adsorption of lysed DNA to the abundant clay particles  
446 in SLW<sup>44</sup>. The particulate methane monooxygenase (*pmoA*) gene clone libraries were  
447 constructed by PCR amplification using A189F (5' GGNGACTGGGACTTCTGG 3') and  
448 m680R (5' CCGGMGCAACGTCYTTACC 3')<sup>24</sup>. The PCR was set up using 0.13  $\mu\text{L}$  of ExTaq  
449 at 5 units  $\mu\text{L}^{-1}$  (Takara), 2.5  $\mu\text{L}$  of 10x ExTaq buffer (Takara), 2  $\mu\text{L}$  dNTP mixture at 2.5mM per  
450 nucleotide (Takara), 2.5  $\mu\text{L}$  of A189F and Mb661R primers (10 pmol  $\mu\text{L}^{-1}$ ), 2  $\mu\text{L}$  molecular  
451 biology-grade bovine serum albumen (BSA; 1.6 mg  $\text{ml}^{-1}$  final concentration) (New England  
452 BioLabs Inc.), 4  $\mu\text{L}$  of template DNA (0.01-0.09 ng DNA  $\mu\text{L}^{-1}$ ), and 11.37  $\mu\text{L}$  of PCR-grade  
453 water for a final reaction volume of 25  $\mu\text{L}$ . The PCR thermocycling conditions were 1 cycle of  
454 98°C for 2 min; 40 cycles of 98°C for 15 s, 55°C for 1 min, and 72°C for 1 min; followed by a  
455 final 72°C for 7 min. PCR was conducted with DNA extraction blanks and no template blanks  
456 (PCR-grade water) as negative controls. Negative controls were not carried forward for cloning,  
457 as no PCR bands were detected. PCR products were run on a 1.5% agarose gel and the 491  
458 basepair *pmoA* fragment was excised from the gel with sterile razor blade and DNA was purified  
459 using a Wizard SV gel clean-up system (Promega). Cleaned *pmoA* fragments were immediately  
460 ligated and cloned with a TA Cloning kit (Invitrogen). Positive clones were transferred to  
461 LB+ampicillin broth and grown overnight at 37°C, then sequenced (288 total sequenced clones)  
462 (Functional Bioscience). The *pmoA* DNA sequences were processed by removing the forward  
463 and reverse primer sequences and removing poor quality sequences (<20 phred score)<sup>50</sup>. Quality  
464 controlled *pmoA* sequences (176 total) were clustered into operational taxonomic units (OTUs) at

465 the 97% similarity level and one representative sequence from each OTU<sup>51</sup>, along with  
466 representative *pmoA* sequences from type Ia and II methanotrophs<sup>24</sup>, were aligned using  
467 ClustalW using the default alignment parameters within the program MEGA6<sup>52</sup>. A phylogenetic  
468 tree was built using the neighbor-joining method with 1000 bootstrap replications<sup>52</sup>. The *pmoA*  
469 sequences have been deposited in GenBank under accession numbers KX589304-KX589461 and  
470 KX784213-KX84230.

471 We attempted to amplify *mcrA* gene sequences from SLW sediment DNA extracts using  
472 a primer set designed to amplify the diversity of *mcrA*-containing methanogens<sup>18</sup> with a nested  
473 PCR amplification scheme. The primer pair used to detect the *mcrA* gene sequence were mcrIRD  
474 <sup>18</sup>. The primer pair is capable of detecting a wide diversity of known and several novel *mcrA*  
475 gene clusters<sup>18</sup>. The first reaction was set up using 0.13  $\mu\text{L}$  of Takara ExTaq at 5 units  $\mu\text{L}^{-1}$ , 2.5  
476  $\mu\text{L}$  10x ExTaq buffer, 2  $\mu\text{L}$  dNTP mixture at 2.5mM per nucleotide (Takara), 2.5  $\mu\text{L}$  of forward  
477 and reverse primer (10 pmol  $\mu\text{L}^{-1}$ ), 2  $\mu\text{L}$  of BSA (1.6 mg  $\text{ml}^{-1}$  final concentration), 9.38  $\mu\text{L}$  PCR-  
478 grade water and 4  $\mu\text{L}$  DNA extract (0.01-0.09 ng DNA  $\mu\text{L}^{-1}$ ) for a final reaction volume of 25  
479  $\mu\text{L}$ . This first reaction was run with an initial denaturation step at 98°C for 2 minutes followed  
480 by 40 cycles of 98°C for 15 s, 53°C for 1 min and 72°C for 1 min, and a final elongation at 72°C  
481 for 7 min. The second reaction was set up using 0.25  $\mu\text{L}$  Takara ExTaq, 5  $\mu\text{L}$  10x ExTaq buffer,  
482 4  $\mu\text{L}$  dNTP mixture at 2.5mM per nucleotide (Takara), 5  $\mu\text{L}$  of forward and reverse primers (10  
483 pmol  $\mu\text{L}^{-1}$ ), 4  $\mu\text{L}$  of BSA (1.6 mg  $\text{ml}^{-1}$  final concentration), 21.75  $\mu\text{L}$  of PCR-grade water and 4  
484  $\mu\text{L}$  of product from the first reaction as template DNA. The second reaction was run with the  
485 same thermocycler program as the first reaction. PCR was conducted with DNA extraction  
486 blanks and no template blanks (PCR-grade water) as negative controls. Details of the 16S rRNA  
487 molecule sample collection and preservation, extraction, reverse transcription, sequencing and

488 processing are described in ref. 21. Extraction blanks were conducted, processed and analyzed in  
489 parallel with the SLW sediment samples as described in ref. 21.

490 **Chemical Affinity Calculations.** An assessment of CH<sub>4</sub> as a potential chemical energy  
491 source for the surficial (0-2 cm) sediment layer was undertaken. The chemical affinity of coupled  
492 oxidation-reduction reactions involving CH<sub>4</sub> and other potential metabolic reactions was  
493 determined. The chemical affinity ( $A_r$ ) is the maximum amount of energy that can be obtained  
494 for a reaction based on *in situ* conditions.  $A_r$  is defined as the change in the overall Gibbs energy  
495 under non-equilibrium conditions ( $\Delta G_r^o$ ) with a change in the progress of the reaction, which  
496 quantifies the reactions proximity to equilibrium<sup>30,31</sup> and is given by;

$$497 \quad A_r = RT \ln(K_r/Q_r) \quad (S1)$$

498 where,  $K_r$  is the calculated equilibrium constant for the reaction, which is derived from  $\Delta G_r^o$  of  
499 the reaction according to  $\Delta G_r^o = G_f^o \text{ products} - G_f^o \text{ reactants}$ , where  $G_f^o$  is the standard Gibbs  
500 energy of formation for the products and reactants<sup>53</sup>.  $K_r$  is given by;

$$501 \quad K_r = e^{-\Delta G_r^o/RT} \quad (S2)$$

502 where R is the gas constant 0.008314 kJ mol<sup>-1</sup>, and T is SLW temperature in Kelvin [-0.5°C =  
503 272.65 K]<sup>53</sup>. Thermodynamic values were derived from ref. 31 using values for 2°C, the closest  
504 available values for the temperature of SLW (-0.5°C); the impact of the temperature difference  
505 on  $\Delta G_r^o$  and resulting  $K_r$  values will be small<sup>30,31</sup>.

506  $Q_r$  is the activity product for the reaction, determined as;

$$507 \quad Q_r = \prod_i (a_i)^{v_{i,r}} \quad (S3)$$

508 where  $a_i$  represents the activity of the i<sup>th</sup> compound in the reaction raised to its stoichiometric  
509 coefficient in the r<sup>th</sup> reaction,  $v_{i,r}$ , which is positive for products and negative for reactants.

510 Activities are calculated from molal concentrations ( $m_i$ ) using activity coefficients ( $\gamma$ ) and the



511 relationship  $a_i = m_i \gamma_i^{30}$ . These activities were calculated using the geochemical model  
512 PHREEQCi<sup>54</sup> using the empirical SLW geochemistry<sup>7,14</sup>. The O<sub>2</sub> concentration in the 0-2 cm  
513 layer was not measured, but for the chemical affinity calculations we consider two scenarios of  
514 O<sub>2</sub> concentration set at 50% (36.5 μM) and 10% (7.3 μM) of average SLW lake water to account  
515 for the decrease in sedimentary O<sub>2</sub> concentration due to consumption and diffusion<sup>55</sup>. Given that  
516 oxygen is inferred to penetrate to ~16cm based on redox sensitive trace metal concentrations<sup>14</sup>, it  
517 is reasonable to model chemical affinity using these two concentrations of O<sub>2</sub> in the surficial  
518 sediment. Temperature, pH, redox (pE) and concentrations of acetate, formate (Supplementary  
519 Fig. 1), dissolved inorganic carbon (DIC), O<sub>2</sub>(aq), CH<sub>4</sub>(aq), SO<sub>4</sub><sup>2-</sup>, NO<sub>3</sub><sup>-</sup>, NH<sub>4</sub><sup>+</sup>, total dissolved  
520 Fe, Ca<sup>2+</sup>, Mg<sup>2+</sup>, Na<sup>+</sup>, K<sup>+</sup>, P, Li<sup>+</sup>, Br<sup>-</sup>, Cl<sup>-</sup> and F<sup>-</sup> were defined<sup>7,14,32,48</sup>. Redox sensitive elements  
521 that were measured as total dissolved elemental concentration (i.e. C, Fe) were assumed to be  
522 speciated to the redox states and species activities as determined by PHREEQC. Conversely,  
523 ions measured in specific redox states (i.e. SO<sub>4</sub><sup>2-</sup>, NO<sub>3</sub><sup>-</sup>, NH<sub>4</sub><sup>+</sup>) were maintained in their  
524 respective redox states by the model, and the species activities including these ions were  
525 calculated.

526 The chemical affinities are expressed in per electron yields ( $A_r^{e^-}$ ) and also shown in terms  
527 of energy density, the energy per kg H<sub>2</sub>O ( $A_r^{kg}$ ), which scales the energy availability to the  
528 limiting reactant, calculated as;

$$529 \quad A_r^{kg} = \left| \frac{A_r}{\nu_i} \right| [i] \quad (S4)$$

530 where,  $[i]$  refers to the concentration of the limiting electron donor or acceptor<sup>56</sup>. This scaling  
531 [equation (S4)] of chemical affinity has been shown to better correlate with actual microbial  
532 communities and metabolisms than the chemical affinity normalized to moles of electrons  
533 transferred<sup>56,57</sup>.

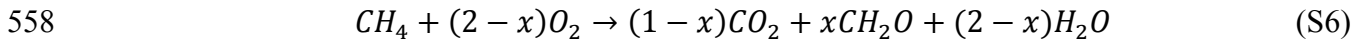
534 **Methane Oxidation Rate Modeling.** CH<sub>4</sub> oxidation rates were modeled by calculating  
535 the flux of CH<sub>4</sub> into the 0-2 cm sediment layer. The CH<sub>4</sub> concentration gradient was determined  
536 using CH<sub>4</sub> values from 15 cm to 3 cm. The flux was calculated using Fick's first law and the  
537 error of the flux determined from the error associated with the diffusional gradient. Water  
538 content was measured and calculated by weighing a known volume of wet weight sediment, then  
539 measuring the sediment again after drying at 95°C for three days<sup>42,47</sup>. Porosity was calculated  
540 from the water content and density of the sediment<sup>42,47</sup>. The diffusion coefficient for CH<sub>4</sub> at 0°C  
541 was corrected for porosity (Supplementary Fig. 3) and tortuosity of SLW sediments calculated  
542 according to equation 3.11 from ref. 58 with C=2.02<sup>58,59</sup>. We modeled the rate of biological CH<sub>4</sub>  
543 consumption according to equation (1) (See main text).

544 The control volume of our model can be defined by the relationship;

$$545 \quad V = A \times H_L + (H_{SS} \times \varphi) \quad (S5)$$

546 where, H<sub>L</sub> and H<sub>SS</sub> are the height of the lake and surficial sediments, respectively, and  $\varphi$  is the  
547 sediment porosity. Assuming steady-state conditions (i.e.,  $\frac{dC}{dt} = 0$ ) and substitution of equation  
548 (S5) into equation (1), R can be calculated as shown in equation (2). R represents the sum of both  
549 microbial CH<sub>4</sub> oxidation to CO<sub>2</sub> and incorporation of CH<sub>4</sub> into biomass. We estimated the  
550 amount of CH<sub>4</sub> removal due to oxidation and incorporation of biomass by assuming that the  
551 biomass partitioning factor, of CH<sub>4</sub> going to biomass is 0.5 [ $x$ ; equation (S6)]. The value of 0.5  
552 has been shown to be a good approximation for the fraction of biomass incorporated by type I  
553 methanotrophs during CH<sub>4</sub> oxidation and is a median value across many habitats<sup>33,60,61</sup>. We  
554 calculated the impact of varying  $x$  from 0.06 to 0.77<sup>36</sup> on biomass C production and  
555 methanotrophy oxygen demand (Supplementary Table 1). From the CH<sub>4</sub> removal rate and the

556 fraction of CH<sub>4</sub> incorporated into biomass, we can then calculate the O<sub>2</sub> consumption by CH<sub>4</sub>  
557 oxidation, which follows the stoichiometric relationship:



559 where  $x$  is the fraction of CH<sub>4</sub> partitioned into biomass formation<sup>33,60,62</sup>. The inputs of O<sub>2</sub> to the  
560 lake are from atmospheric gases released by melting of the overlying meteoric ice and advection  
561 of water into the lake during the filling phase of the hydrologic cycle<sup>9,32,63</sup>. Based on the  
562 concentration of gas in the overlying ice and the basal ice melt rate, which has been estimated at  
563 1.8 cm yr<sup>-1</sup> (ref. 9), the overlying ice sheet supplies 1.0 x 10<sup>6</sup> mol O<sub>2</sub> yr<sup>-1</sup> (67% of O<sub>2</sub> supply to  
564 SLW)<sup>32</sup>. Advection into the lake provides 5 x 10<sup>5</sup> mol O<sub>2</sub> yr<sup>-1</sup> (33% of O<sub>2</sub> supply to SLW)<sup>32</sup>,  
565 assuming the incoming water has the same concentration measured in the SLW water  
566 column<sup>32,63</sup>. When the fraction of carbon from CH<sub>4</sub> going to biomass is varied (Supplementary  
567 Table 1), the oxygen demand on the system changes as well. We used the SLW oxygen budget  
568 from ref. 32 to determine the impact of the biomass partitioning factor ( $x$ ) could have on the  
569 oxygen demand for biological processes in SLW (Supplementary Table 1).

570 **Data availability.** Data generated for this study are available through the microbial  
571 Antarctic resource system database (<http://mars.biodiversity.aq/resources/97>). Molecular data  
572 were accessed from NCBI sequence read archive (<https://www.ncbi.nlm.nih.gov/sra>) project  
573 PRJNA244335.

574

## 575 **References**

- 576 40. Priscu, J. C. *et al.* A microbiologically clean strategy for access to the Whillans Ice Stream  
577 subglacial environment. *Antarct. Sci.* **11**, 1–11 (2013).
- 578 41. Tulaczyk, S. *et al.* WISSARD at Subglacial Lake Whillans, West Antarctica: scientific

- 579 operations and initial observations. *Ann. Glaciol.* **55**, 51–58 (2014).
- 580 42. Riedinger, N. *et al.* Methane at the sediment–water transition in Black Sea sediments.  
581 *Chem. Geol.* **274**, 29–37 (2010).
- 582 43. Yarnes, C.  $^{13}\text{C}$  and  $^2\text{H}$  measurement of methane from ecological and geological sources by  
583 gas chromatography/combustion/pyrolysis isotope-ratio mass spectrometry. *Rapid*  
584 *Commun. Mass Spectrom.* **27**, 1036–1044 (2013).
- 585 44. Lever, M. A. *et al.* A modular method for the extraction of DNA and RNA, and the  
586 separation of DNA pools from diverse environmental sample types. *Front. Microbiol.* **6**,  
587 1–25 (2015).
- 588 45. National Resource Council. *Exploration of Antarctic Subglacial Aquatic Environments*.  
589 (The National Academies Press, 2007).
- 590 46. Wiesenburg, D. A. & Guinasso Jr., N. L. Equilibrium solubilities of methane, carbon  
591 monoxide, and hydrogen in water and sea water. *J. Chem. Eng. Data* **24**, 356–360 (1979).
- 592 47. Avnimelech, Y., Ritvo, G., Meijer, L. E. & Kochba, M. Water content, organic carbon and  
593 dry bulk density in flooded sediments. *Aquac. Eng.* **25**, 25–33 (2001).
- 594 48. Vick-Majors, T. J. Biogeochemical processes in Antarctic aquatic environments: Linkages  
595 and limitations. (Montana State University, 2016).
- 596 49. Solorzano, L. Determination of ammonia in natural waters by the phenolhypochlorite  
597 method. *Limnol. Oceanogr.* **14**, 799–801 (1969).
- 598 50. Paegel, B. M., Emrich, C. A., Wedemayer, G. J., Scherer, J. R. & Mathies, R. A. High  
599 throughput DNA sequencing with a microfabricated 96-lane capillary array  
600 electrophoresis bioprocessor. *Proc. Natl. Acad. Sci.* **99**, 574–579 (2002).
- 601 51. Schloss, P. D. *et al.* Introducing mothur: Open-source, platform-independent, community-

- 602 supported software for describing and comparing microbial communities. *Appl. Environ.*  
603 *Microbiol.* **75**, 7537–7541 (2009).
- 604 52. Tamura, K., Stecher, G., Peterson, D., Filipski, A. & Kumar, S. MEGA6: Molecular  
605 evolutionary genetics analysis version 6.0. *Mol. Biol. Evol.* **30**, 2725–2729 (2013).
- 606 53. Stumm, W. & Morgan, J. J. *Aquatic Chemistry: Chemical Equilibria and Rates in Natural*  
607 *Waters*. (Wiley-Interscience, 1996).
- 608 54. Parkhurst, D. L. & Appelo, C. A. J. in *U.S. Geological Survey Techniques and Methods*  
609 497 (US Geological Survey, 2013).
- 610 55. Boetius, A. & Wenzhöfer, F. Seafloor oxygen consumption fuelled by methane from cold  
611 seeps. *Nat. Geosci.* **6**, 725–734 (2013).
- 612 56. LaRowe, D. E. & Amend, J. P. in *Microbial Life of the Deep Biosphere* (eds. Kallmeyer,  
613 J. & Wagner, D.) 279–302 (Walter de Gruyter, 2014).
- 614 57. Osburn, M. R. *et al.* Chemolithotrophy in the continental deep subsurface: Sanford  
615 Underground Research Facility (SURF), USA. *Front. Microbiol.* **5**, 1–14 (2014).
- 616 58. Shen, L. & Chen, Z. Critical review of the impact of tortuosity on diffusion. *Chem. Eng.*  
617 *Sci.* **62**, 3748–3755 (2007).
- 618 59. Broecker, W. S. & Peng, T.-H. Gas exchange rates between air and sea. *Tellus* **26**, 21–35  
619 (1974).
- 620 60. Shelley, F., Abdullahi, F., Grey, J. & Trimmer, M. Microbial methane cycling in the bed  
621 of a chalk river: oxidation has the potential to match methanogenesis enhanced by  
622 warming. *Freshw. Biol.* **60**, 150–160 (2015).
- 623 61. Whalen, S. C., Reeburgh, W. S. & Sandbeck, K. A. Rapid Methane Oxidation in a  
624 Landfill Cover Soil. *Appl. Environ. Microbiol.* **56**, 3405–3411 (1990).

- 625 62. Urmann, K., Lazzaro, A., Gandolfi, I., Schroth, M. H. & Zeyer, J. Response of  
626 methanotrophic activity and community structure to temperature changes in a diffusive  
627 CH/O counter gradient in an unsaturated porous medium. *FEMS Microbiol. Ecol.* **69**,  
628 202–12 (2009).
- 629 63. Siegfried, M. R., Fricker, H. A., Carter, S. P. & Tulaczyk, S. Episodic ice velocity  
630 fluctuations triggered by a subglacial flood in West Antarctica. *Geophys. Res. Lett.* **43**,  
631 2640–2648 (2016).

